Eur. Phys. J. C (2026) 86:762
https://doi.org/10.1140/epjc/s10052-026-16010-6

THE EUROPEAN PHYSICAL JOURNAL C

Regular Article - Theoretical Physics

Revisiting the evidence for dynamical dark energy: from DES-SN5Y to DES-Dovekie

Anil Kandel[1,a], **Farruh Atamurotov**[2,3,4,b], **Ertan Güdekli**[5,c], **Phongpichit Channuie**[6,d], **Gulzoda Rakhimova**[7,e]

[1] Department of Physics, St. Xavier's College, Tribhuvan University, Kathmandu, Nepal
[2] Kimyo International University in Tashkent, Shota Rustaveli str. 156, Tashkent 100121, Uzbekistan
[3] National University of Uzbekistan, Tashkent 100174, Uzbekistan
[4] Research Center of Astrophysics and Cosmology, Khazar University, 41 Mehseti Street, Baku AZ1096, Azerbaijan
[5] Department of Physics, Faculty of Science, Istanbul University, 34134 Istanbul, Turkey
[6] School of Science and College of Graduate Studies, Walailak University, Nakhon Si Thammarat 80160, Thailand
[7] University of Tashkent for Applied Sciences, Str. Gavhar 1, 100149 Tashkent, Uzbekistan

Received: 2 April 2026 / Accepted: 16 June 2026
© The Author(s) 2026

Abstract Recent analyses combining DESI DR2 BAO measurements with CMB and supernova data have suggested a preference for dynamical dark energy, particularly when using the DES-SN5Y and DES-SN5Y ($z > 0.1$) supernova samples. With the revision of this dataset into the DES-Dovekie compilation, it is important to reassess the robustness of this result. In this work, we analyze a broad class of dark energy parametrizations, including wCDM, w_0w_aCDM, BA, JBP, Efstathiou, and GEDE models, using DESI DR2 BAO, a compressed CMB likelihood, and supernova data. We find that the DES-SN5Y dataset consistently yields a stronger preference for deviations from ΛCDM compared to DES-Dovekie. In particular, redshift-dependent parametrizations favor the region $w_0 > -1$ and $w_a < 0$, corresponding to a Quintom-B–type evolution with phantom crossing. This behavior is observed across multiple models, indicating that it is not specific to a single parametrization. We find that the DES-SN5Y ($z > 0.1$) sample also preserves the same qualitative behavior, although the deviations from the ΛCDM limit become significantly weaker compared to the full DES-SN5Y sample. However, when DES-Dovekie is used, the statistical preference for dynamical dark energy is significantly reduced. The improvement over ΛCDM drops to below the 1σ level for most models, and the Bayesian evidence weakens from moderate to weak or inconclusive. Similarly, for the DES-SN5Y ($z > 0.1$) sample, the preference for dynamical dark energy becomes intermediate between the DES-SN5Y and DES-Dovekie cases, with mostly weak or inconclusive evidence. Overall, the DES-Dovekie and DES-SN5Y ($z > 0.1$) datasets weaken the preference for dynamical dark energy compared to the full DES-SN5Y dataset.

1 Introduction

One of the most striking discoveries of modern astrophysics is that, contrary to earlier expectations that cosmic expansion would decelerate due to gravity, the expansion of the universe is actually accelerating. This acceleration was revealed in the late 1990s through observations of Type Ia supernovae [1,2], leading to the introduction of dark energy as the primary driver of this phenomenon. Follow-up observations of the cosmic microwave background (CMB) anisotropies [3,4] have provided robust confirmation of this cosmological framework, delivering precise measurements of the universe's energy composition and showing that dark energy makes up nearly 70% of the total energy density. These observations support the Λ cold dark matter (ΛCDM) model, confirming Λ as the cosmological constant and CDM as the primary form of cold dark matter.

Emerging evidence in cosmology challenges the assumption of a constant dark energy component, instead pointing toward a dynamically evolving one. In particular, studies of baryon acoustic oscillation (BAO) measurements from dark

[a] e-mail: anil.kandel3227@gmail.com
[b] e-mail: atamurotov@yahoo.com
[c] e-mail: gudekli@istanbul.edu.tr
[d] e-mail: phongpichit.ch@mail.wu.ac.th (corresponding author)
[e] e-mail: rakhimovagulzoda96@gmail.com

Published online: 03 July 2026

energy spectroscopic instrument (DESI) Data Release 1 suggest a preference for a dynamical dark energy (DDE) component over the cosmological constant, with a statistical significance of 2.6σ for the DESI DR1 + CMB combination. This preference persists and even strengthens when Type Ia supernovae (SNe Ia) datasets are included, leading to tensions with the ΛCDM model at the 2.5σ, 3.5σ, and 3.9σ levels for the Pantheon$^+$, Union3, and dark energy survey (DES) 5-year sample of Type Ia supernovae (DES-SN5Y) compilations, respectively [5]. Furthermore, incorporating the latest DESI DR2 data provides additional support for this behaviour, yielding a preference for DDE at the 3.1σ level for the DESI DR2 + CMB combination. When combined with SNe Ia datasets, the exclusion significance of the ΛCDM model increases to 2.8σ, 3.8σ, and 4.2σ for the Pantheon$^+$, Union3, and DES-SN5Y samples, respectively[6]. Recently, a re-analysis of the DES-SN5Y sample, referred to as the DES-Dovekie dataset, shows that the preference for DDE decreases to a statistical significance of 3.2σ, compared to 4.2σ for the original DES-SN5Y sample. In the context of DESI DR2, several recent studies further support this behaviour, as discussed in [7–21].

Beyond the possibility of DDE, persistent cosmological tensions arise when the ΛCDM model is tested against various observational data sets [22,23]. Among these, the most notable and statistically robust is the Hubble tension. Current estimates of the Hubble constant (H_0) derived from CMB observations [24–26], under the assumption of the ΛCDM framework, are in excess of 5σ disagreement with values obtained from direct astrophysical measurements [27].

A key quantity used to describe the physical properties of dark energy is the equation of state (EoS) parameter, commonly denoted by w. It is defined as the ratio of pressure p to the corresponding energy density ρ. This parameter plays an important role in determining the dynamical behavior of dark energy throughout cosmic evolution. In the standard cosmological framework, dark energy is often modeled by the cosmological constant Λ, which corresponds to a constant equation of state $w = -1$. Despite its simplicity and observational success, the cosmological constant scenario suffers from significant theoretical issues, most notably the fine-tuning problem [28]. Various theoretical scenarios consider a time-dependent equation of state, $w(z)$, where z denotes the redshift, allowing dark energy to evolve dynamically over cosmic time. Prominent examples include quintessence models [29,30], phantom field models [31], and quintom models [32]. Constraining the evolution of $w(z)$ through observational data is therefore essential for distinguishing among these theoretical frameworks. Several parameterizations of $w(z)$ are considered in this work.

As discussed earlier, the preference for DDE decreases when moving from the DES-SN5Y sample to the revised DES-Dovekie dataset. Motivated by this behavior, in this work we perform a systematic analysis of several DDE models using the latest DESI DR2 data in combination with the SNe Ia from the DES-Dovekie and DES-SN5Y supernova compilations. In addition, we also investigate the possible deviation toward DDE within the DES-SN5Y sample itself. For this purpose, we remove the low-redshift supernovae from the DES-SN5Y sample ($z < 0.1$), since they may introduce significant uncertainties due to the influence of peculiar velocities, which can dominate over the Hubble flow and bias cosmological parameter inference. This also allows us to examine whether the preference for DDE becomes weaker after excluding the very low-redshift supernovae. Apart from this, we also consider several dark energy parametrizations to examine whether this behavior of dynamical dark energy arises only because of the choice of a single parametrization or represents a more general feature across different dark energy models.

Our paper is organized as follows. In Sect. 2, we introduce the cosmological background equations and dark energy models. In Sect. 3, we introduce methodology and datasets using the Markov Chain Monte Carlo (MCMC) sampling against the publicly available DESI DR2 data, while Sect. 4 is dedicated to the discussion of results. In Sect. 5, we draw the conclusions.

2 Background equations and dark energy models

We work within the framework of a spatially flat Friedmann–Lemaître–Robertson–Walker metric spacetime, which provides an appropriate description of the homogeneous and isotropic universe on large scales. The corresponding line element is expressed as

$$ds^2 = -dt^2 + a^2(t)[dr^2 + r^2(d\theta^2 + \sin^2\theta d\phi^2)], \tag{1}$$

where $a(t)$ is the scale factor that describes the cosmic expansion as a function of time and (r,θ,ϕ) are the standard spherical coordinates. The Einstein field equation

$$G_{\mu\nu} = 8\pi G\, T^{(m)}_{\mu\nu}, \tag{2}$$

leads to the Friedmann equations. The first Friedmann equation, neglecting the radiation contribution, is

$$H^2 = \frac{8\pi G}{3}\left(\rho_{\rm m} a^{-3} + \rho_{\rm de}\right). \tag{3}$$

where $T^{(m)}_{\mu\nu}$ is the standard matter-energy component, $G_{\mu\nu} = R_{\mu\nu} - g_{\mu\nu}R/2$ is the Einstein tensor, and G is the Newtonian gravitational constant. In the FLRW background, the continuity equation takes the form

$$\dot{\rho}_{\rm x} + 3H(1 + w_{\rm x})\rho_{\rm x} = 0, \tag{4}$$

where ρ_x represents the energy density of each component with x$\in$ (matter, DE), over $\dot{()}$ represents the cosmic time derivative, and w_x represents the equation of state parameter (EoS). The dimensionless Hubble parameter $E(z) = H(z)/H_0$, where $H(z) = \dot{a}/a$ and H_0 is the present-day value, determines the expansion history of the Universe. From Eq. (3), $E(z)^2$ is:

$$E(z)^2 = \Omega_m(1+z)^3 + \Omega_\Lambda f_{\rm DE}(z), \tag{5}$$

where Ω_m, and Ω_Λ are the present-day fractional energy densities of matter and DE, respectively. Also, f_{DE} represents the evolution of DE.

The evolution of DE ($\rho_{\rm de}$) within Eq. (3) will be the following solution of Eq. (4):

$$f_{\rm DE}(z) \equiv \frac{\rho_{\rm de}(z)}{\rho_{\rm de,0}} = \exp\left[3\int_0^z \frac{1+w(z')}{1+z'}\,dz'\right] \tag{6}$$

Here, $\rho_{\rm de,0}$ represents the current dark energy density. For $w = -1$ corresponding to a positive cosmological constant (Λ), the right-hand side of Eq. (6) becomes unity, and Eq. (5) reduces to the conventional expression.

We consider the following EoS parameterizations:

- *Chevallier Polarski Linder (CPL)* [33,34]

  $w(z) = w_0 + \frac{z}{1+z}\,w_a$
- *Barboza Alcaniz (BA)* [35]

  $w(z) = w_0 + \frac{z(1+z)}{1+z^2}\,w_a$
- *Jassal Bagla Padmanabhan (JBP)* [36]

  $w(z) = w_0 + \frac{z}{(1+z)^2}\,w_a$
- *Efstathiou* [37]

  $\omega(z) = w_0 + w_a \ln(1+z)$
- *Generalized Emergent Dark Energy (GEDE)* [38]

  $w(z) = -1 - \frac{\Delta}{3\ln 10}\left[1 + \tanh\left(\Delta \log_{10}\left(\frac{1+z}{1+z_t}\right)\right)\right]$

For any given $w(z)$, the function $f_{\rm DE}(z)$ is obtained from Eq. (6); substituting this into Eq. (5) provides corresponding expansion history $E(z)$.

3 Methodology and data

In our analysis, we use the `SimpleMC`[1] cosmological inference code to estimate the posterior distributions of parameters for each cosmological model. To assess the convergence of our chains, we use the Gelman-Rubin statistic $(R-1)$, adopting $(R-1) < 0.01$ as the threshold for convergence [39]. The MCMC results are analyzed and visualized using `getdist` [40]. We then constrain the models using a combination of the following datasets: BAO measurements from DESI DR2, compressed *CamSpec* CMB likelihood, and SNe Ia samples, including DES-SN5YR and DES-Dovekie, a more detailed description of the datasets is given below.

- *Baryon Acoustic Oscillation:* We incorporate the latest BAO measurements from the second Data Release (DR2) of the DESI survey [41]. These data are obtained using multiple tracers, including the Bright Galaxy Sample (BGS), Luminous Red Galaxies (LRG1–3), Emission Line Galaxies (ELG1–2), Quasars (QSO), and the Lyman-α forest. This includes measurements from over 13.1 million galaxies and 1.6 million quasars, covering the redshift range $0.295 \le z \le 2.330$. It is necessary to derive the transverse comoving distance D_M/r_d, the Hubble horizon D_H/r_d, the angle-averaged distance D_V/r_d, and D_M/D_H to constrain the parameters of each model, where r_d is the comoving sound horizon at the drag epoch. In flat ΛCDM, it is given by $r_d = 147.09 \pm 0.2$ Mpc [42].
- *Type Ia supernovae:* We use the DES-SN5Y compilation, which consists of 1829 SNe Ia, including 1635 photometrically classified SNe Ia at $z > 0.1$ with uniform calibration from a single survey extending up to $z = 1.13$, together with an additional set of 194 SNe Ia at $z < 0.1$ [43]. As we know, low-redshift supernovae, particularly those with $z < 0.1$, may introduce significant uncertainties due to the effects of peculiar velocities, which can dominate over the Hubble flow and potentially bias the cosmological parameter inference [44,45]. Therefore, we apply the cut $z > 0.1$ to the DES-SN5Y sample, which we denote as DES-SN5Y ($z > 0.1$). We also use the DES-Dovekie dataset, a newly SNe Ia derived from a recalibration and comprehensive re-analysis of the DES-SN5YR dataset, which contains a total of 1820 SNe Ia [46].
- *CMB compressed likelihood:* Finally, we use the compressed *CamSpec* CMB likelihood, given as a 3×3 Gaussian likelihood for $\{\theta_*, \omega_b, \omega_{bc}\}$. Here, θ_* denotes the angular size of the sound horizon at recombination, and ω_b and ω_{bc} are the physical baryon and total matter densities, respectively. Since $\theta_* \propto r_s(z_*)/D_M(z_*)$, fixing $r_s(z_*)$ (assuming ΛCDM prior to recombination) allows θ_* to constrain $D_M(z_*)$, while ω_{bc} constrains the matter density. For further details, we refer the reader to Appendix A of [41].

[1] https://github.com/ja-vazquez/SimpleMC.git..

Table 1 The parameters and their priors including uniform priors $\mathcal{U}$ and the reduced Hubble constant $h \equiv H_0/100$, where H_0 is expressed in units of $\mathrm{km\,s^{-1}\,Mpc^{-1}}$

Parametrization	Parameter	Prior
ΛCDM	h	$\mathcal{U}[0.4, 0.9]$
	$\Omega_b h^2$	$\mathcal{U}[0.02, 0.025]$
	Ω_m	$\mathcal{U}[0.1, 0.5]$
Dark energy	w or w_0	$\mathcal{U}[-3, 1]$
	w_a	$\mathcal{U}[-3, 2]$
Emergent	Δ	$\mathcal{U}[-3, 10]$

Finally, we also use the bayesian evidence criterion to evaluate whether dark energy (DE) models are statistically favored over the ΛCDM model. The Bayesian evidence, Z, is defined as the integral of the likelihood across the prior parameter space,

$$Z = \int_\Omega \mathcal{L}(\theta)\,\pi(\theta)\,d\theta, \tag{7}$$

where $\mathcal{L}(\theta) \equiv P(D|\theta, M)$ is the likelihood of the data D given the parameters θ and model M, and $\pi(\theta) \equiv P(\theta|M)$ is the prior distribution of the parameters within that model. To compare two competing models, we compute the Bayes factor in logarithmic form,

$$\ln \mathcal{B}_{ij} = \ln Z_i - \ln Z_j, \tag{8}$$

where $\ln Z_i$ and $\ln Z_j$ denote the Bayesian evidences of models i and j, respectively. To interpret the strength of the evidence, we adopt the revised Jeffreys' scale [47,48]. According to this criterion, the strength of evidence can be interpreted as follows: $\ln \mathcal{B}_{ij} < 1$ indicates inconclusive evidence; $1 \leq \ln \mathcal{B}_{ij} < 2.5$ suggests weak evidence; $2.5 \leq \mathcal{B}_{ij} < 5$ corresponds to moderate evidence; $5 \leq \mathcal{B}_{ij} < 10$ signifies strong evidence; and $\ln \mathcal{B}_{ij} \geq 10$ denotes decisive evidence. In this analysis, we use several DE models, with the chosen priors summarized in Table 2.

The chosen priors for the ΛCDM model, each dark energy model, and the emergent dark energy model are summarized in Table 1.

4 Results

In this section, we explore different dark energy models and investigate the preference for DDE over the cosmological constant. The main motivation comes directly from the DESI DR2 results. When combined with CMB, DESI DR2 BAO, and DES-SN5Y SNe Ia dataset, this combination shows a preference for DDE up to 4.2σ. However, the DES-SN5Y SNe Ia dataset was later revised with the introduction of the new DES–Dovekie dataset, where the significance reduces to about 3.2σ. In addition, we also consider the DES-SN5Y sample by applying the cut $z > 0.1$, in order to examine the impact of the low-redshift supernovae on the dark energy constraints.

Indeed, in that analysis, only the $w_0 w_a$CDM model was explored. Here, we extend the study beyond this framework by considering more dark energy parameterizations such as BA, JBP, Efstathiou, and GEDE models, in order to examine whether this behavior is driven specifically by the $w_0 w_a$CDM model or represents a more general feature of DDE.

In Table 2, we show the mean values and their corresponding uncertainties at the 1σ confidence level. We observe a clear difference between the DES-SN5Y and DES-Dovekie supernova samples. In general, the DES-SN5Y dataset shows a larger preference for DDE compared to DES-Dovekie across all models. In the wCDM model, the value shifts from $w = -0.964 \pm 0.025$ (DES-Dovekie) to $w = -0.945^{+0.025}_{-0.023}$ (DES-SN5Y), with the deviation increasing from 1.44σ to 2.20σ, indicating a stronger preference for deviations from $w = -1$. However, after applying the $z > 0.1$ cut to the DES-SN5Y sample, the constraint becomes $w = -0.988 \pm 0.030$, corresponding to 0.40σ deviation from $w = -1$, showing inconclusive preference for DDE.

A similar trend is seen in each DDE models. In the $w_0 w_a$CDM model, w_0 shifts from -0.865 ± 0.052 to -0.798 ± 0.052, with the significance increasing from 2.60σ to 3.88σ, while w_a shifts from -0.42 ± 0.20 to -0.63 ± 0.21, with the deviation increasing from 2.10σ to 3.00σ. For the DES-SN5Y ($z > 0.1$) sample, we get $w_0 = -0.87 \pm 0.11$, corresponding to a deviation of only 1.18σ from $w = -1$. For the BA model, w_0 shifts from -0.876 ± 0.054 to $-0.841^{+0.049}_{-0.044}$, corresponding to an increase from 2.30σ to 3.24σ, while w_a changes from $-0.23^{+0.14}_{-0.13}$ to -0.26 ± 0.10, with the deviation increasing from 1.64σ to 2.60σ. For the DES-SN5Y ($z > 0.1$) sample, we get $w_0 = -0.891^{+0.088}_{-0.10}$, corresponding to a deviation of about 1.16σ. The JBP model shows a similar pattern, where w_0 shifts from -0.785 ± 0.085 to -0.751 ± 0.075, increasing from 2.53σ to 3.32σ, and w_a from -1.14 ± 0.52 to $-1.23^{+0.44}_{-0.49}$, increasing from 2.19σ to 2.51σ. For the DES-SN5Y ($z > 0.1$) sample, we get $w_0 = -0.90 \pm 0.18$, corresponding to only a 0.56σ deviation from $w = -1$.

The Efstathiou model follows the same behavior, with w_0 changing from -0.870 ± 0.050 to -0.816 ± 0.051, increasing from 2.60σ to 3.61σ, and w_a from $-0.34^{+0.18}_{-0.15}$ to -0.46 ± 0.17, with the deviation increasing from 1.89σ to 2.71σ. Using the DES-SN5Y ($z > 0.1$) sample instead gives $w_0 = -0.890 \pm 0.087$, corresponding to a reduced deviation of about 1.26σ. For the GEDE model, the parameter Δ shifts from -0.25 ± 0.18 (DES-Dovekie) to -0.39 ± 0.18 (DES-

Table 2 This table shows the mean values and corresponding errors at the 68% (1σ) confidence level for the ΛCDM, wCDM, w_0w_aCDM, BA, JBP, Logarithmic, and GEDE models, obtained using DESI DR2 measurements in combination with the compressed CMB likelihood and two SNe Ia datasets (DES-Dovekie and DES-SN5Y)

Dataset	h	Ω_m	w or w_0	w_a	Δ	$\ln \mathcal{B}_{\Lambda\text{CDM, model}}$	$\Delta\chi^2_{\text{MAP}}$	$N\sigma$
ΛCDM								
CMB + DESI DR2 + DES-Dovekie	0.6792 ± 0.0045	0.3069 ± 0.0054	–	–	–	0	0	0
CMB + DESI DR2 + DES-SN5Y	0.6775 ± 0.0046	0.3090 ± 0.0057	–	–	—	0	0	0
CMB + DESI DR2 + DES-SN5Y ($z > 0.01$)	0.6814 ± 0.0045	0.3043 ± 0.0055	–	–	–	0	0	0
$wCDM$								
CMB + DESI DR2 + DES-Dovekie	0.6801 ± 0.0059	0.3072 ± 0.0059	-0.964 ± 0.025	–	–	0.39	0.00	0.00
CMB + DESI DR2 + DES-SN5Y	0.6747 ± 0.0061	0.3119 ± 0.0062	$-0.945^{+0.025}_{-0.023}$	–	–	1.67	−4.48	2.12
CMB + DESI DR2 + DES-SN5Y ($z > 0.1$)	0.6860 ± 0.0079	0.3026 ± 0.0073	-0.988 ± 0.030	–	–	−0.18	−2.26	1.50
w_0w_aCDM								
CMB + DESI DR2 + DES-Dovekie	0.6779 ± 0.0063	0.3115 ± 0.0068	-0.865 ± 0.052	-0.42 ± 0.20	–	2.05	−2.17	0.96
CMB + DESI DR2 + DES-SN5Y	0.6726 ± 0.0063	0.3171 ± 0.0067	-0.798 ± 0.052	-0.63 ± 0.21	–	4.87	−8.02	2.36
CMB + DESI DR2 + DES-SN5Y ($z > 0.1$)	0.6780 ± 0.0100	0.6780 ± 0.0100	-0.87 ± 0.11	-0.43 ± 0.35	–	0.50	−2.87	1.18
BA								
CMB + DESI DR2 + DES-Dovekie	0.6783 ± 0.0064	0.3114 ± 0.0067	-0.876 ± 0.054	$-0.23^{+0.14}_{-0.13}$	–	1.35	−2.16	0.95
CMB + DESI DR2 + DES-SN5Y	0.6731 ± 0.0064	0.3161 ± 0.0067	$-0.841^{+0.049}_{-0.044}$	-0.26 ± 0.10	–	4.05	−8.01	2.36
CMB + DESI DR2 + DES-SN5Y ($z > 0.1$)	0.679 ± 0.011	$0.3106^{0.0098}_{-0.011}$	$-0.891^{+0.088}_{-0.10}$	$-0.19^{+0.19}_{-0.16}$	–	−0.24	−2.86	1.18
JBP								
CMB + DESI DR2 + DES-Dovekie	0.6767 ± 0.0063	0.3121 ± 0.0066	-0.785 ± 0.085	-1.14 ± 0.52	–	2.86	−2.11	0.95
CMB + DESI DR2 + DES-SN5Y	0.6715 ± 0.0064	0.3168 ± 0.0068	-0.751 ± 0.075	$-1.23^{+0.44}_{-0.49}$	–	5.47	−8.01	2.36
CMB + DESI DR2 + DES-SN5Y ($z > 0.1$)	0.682 ± 0.013	0.307 ± 0.012	-0.90 ± 0.18	-0.50 ± 0.95	–	1.12	−2.59	1.09
Efstathiou								
CMB + DESI DR2 + DES-Dovekie	0.6788 ± 0.0060	0.3114 ± 0.0064	-0.870 ± 0.050	$-0.34^{+0.18}_{-0.15}$	–	1.80	−2.13	0.94
CMB + DESI DR2 + DES-SN5Y	0.6729 ± 0.0062	0.3176 ± 0.0066	-0.816 ± 0.051	-0.46 ± 0.17	–	4.40	−7.90	2.34
CMB + DESI DR2 + DES-SN5Y ($z > 0.1$)	0.6794 ± 0.0098	0.311 ± 0.010	-0.890 ± 0.087	$-0.28^{+0.25}_{-0.19}$	–	0.01	−2.98	1.21
GEDE								
CMB + DESI DR2 + DES-Dovekie	0.6799 ± 0.006	0.3076 ± 0.0063	–	–	-0.25 ± 0.18	2.67	−0.08	0.28
CMB + DESI DR2 + DES-SN5Y	0.6741 ± 0.0064	0.3126 ± 0.0064	–	–	-0.39 ± 0.18	4.03	−4.64	2.15
CMB + DESI DR2 + DES-SN5Y ($z > 0.1$)	0.6872 ± 0.0086	0.3018 ± 0.0075	–	–	-0.04 ± 0.25	1.89	−2.31	1.52

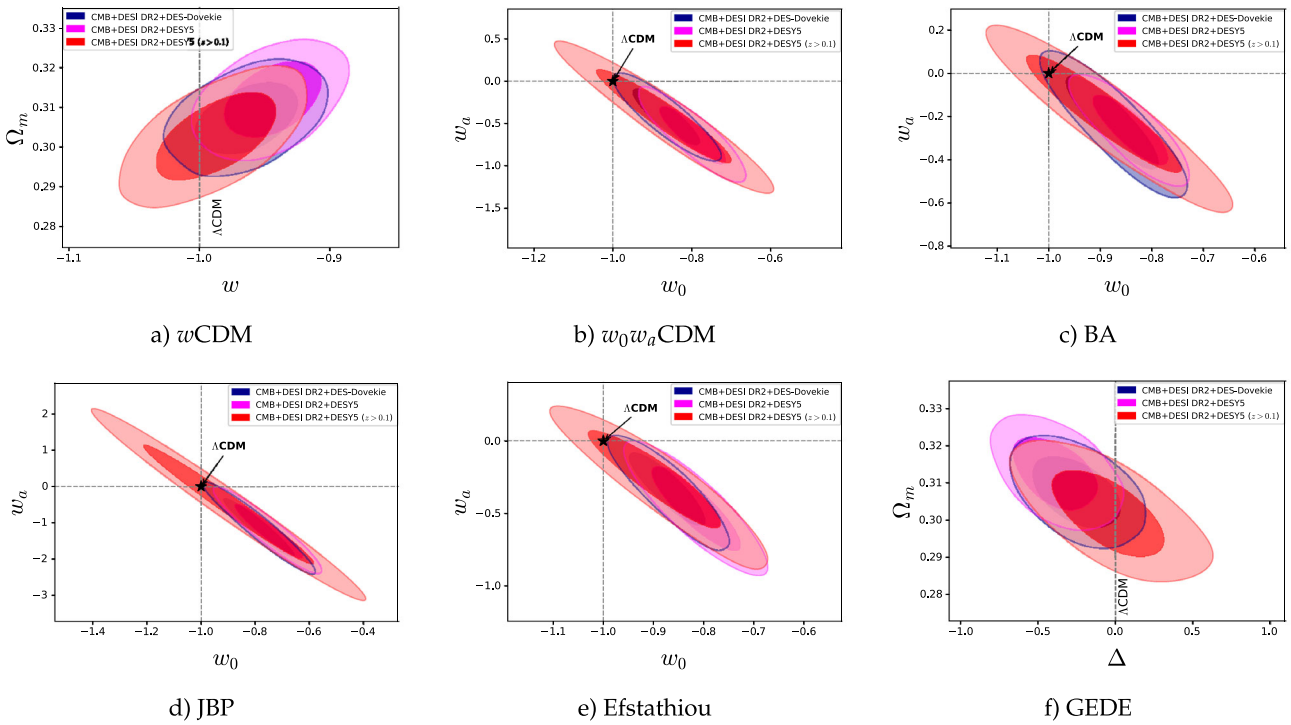


Fig. 1 This figure shows the 2D marginalized confidence contours for the wCDM, w_0w_aCDM, BA, JBP, Efstathiou, and GEDE models, obtained using DESI DR2 measurements in combination with the compressed CMB likelihood andvSNe Ia datasets (DES-Dovekie, DES-SN5Y, and DES-SN5Y ($z > 0.1$)), at the 68% (1σ) and 95% (2σ) confidence levels

SN5Y), with the deviation increasing from 1.39σ to 2.17σ, although it remains smaller compared to the other models. For the DES-SN5Y ($z > 0.1$) sample, the GEDE parameter becomes $\Delta = -0.04 \pm 0.25$, corresponding to only a 0.16σ deviation from the ΛCDM limit. Overall, the DES-SN5Y dataset consistently shows stronger deviations from ΛCDM than DES-Dovekie, suggesting a stronger preference of DDE. However, after excluding the very low-redshift ($z < 0.01$) supernovae, the preference for DDE is significantly weakened across all models, with all deviations reducing to nearly 1σ or below.

4.1 Quintom-B–type dark energy

Figure 1 shows the 2D marginalized confidence contours of the wCDM, w_0w_aCDM, BA, JBP, Efstathiou, and GEDE models at 1σ and 2σ confidence levels. In Fig. 1a, b show the 2D marginalized confidence contours of the $w_0 - w_a$ plane for the w_0w_aCDM, BA, JBP, and Efstathiou models, respectively. It can be observed that in all the cases, each model prefers values in the quadrant $w_0 > -1$ and $w_a < 0$. This region corresponds to a class of dark energy characterized by the Quintom-B scenario ($w_0 > -1$, $w_a < 0$, and $w_0 + w_a < -1$) [49–52]. In this scenario, EoS parameter evolves from $w < -1$ at earlier times to $w > -1$ at the present epoch. Such an evolution involves a transition across $w = -1$, which is commonly referred to as phantom crossing [53–56].

Figure 1f shows the 2D marginalized confidence contours of the $\Delta - \Omega_m$ plane for the GEDE model. It can be observed that in each case, when using the DES-Dovekie, DES-SN5Y, and DES-SN5Y ($z > 0.1$) datasets, the GEDE model consistently prefers $\Delta < 0$ indicating a possible injection of dark energy at high redshifts [15,57,58]. However, for the DES-SN5Y ($z > 0.1$) sample, the value of Δ becomes very close to the ΛCDM limit, i.e. $\Delta = 0$. Indeed, it is interesting to note that $\Delta_{\text{DES-SN5Y}} < \Delta_{\text{DES-Dovekie}}$.

4.2 Preference for dynamical dark energy from DES-SN5Y to DES-Dovekie

In this subsection, we quantify the preference for DDE using the DES-Dovekie, DES-SN5Y, and DES-SN5Y ($z > 0.1$) datasets. To assess this, we use the difference in the best-fit chi-square values between the DDE models and the ΛCDM scenario, $\Delta\chi^2_{\text{MAP}} \equiv \chi^2_{\text{DDE}} - \chi^2_{\Lambda\text{CDM}}$. Since ΛCDM is nested within the broader class of DDE models, $\Delta\chi^2_{\text{MAP}}$ is expected to follow a χ^2 distribution with degrees of freedom equal to the number of additional free parameters in the DDE model, assuming Gaussian uncertainties and ΛCDM

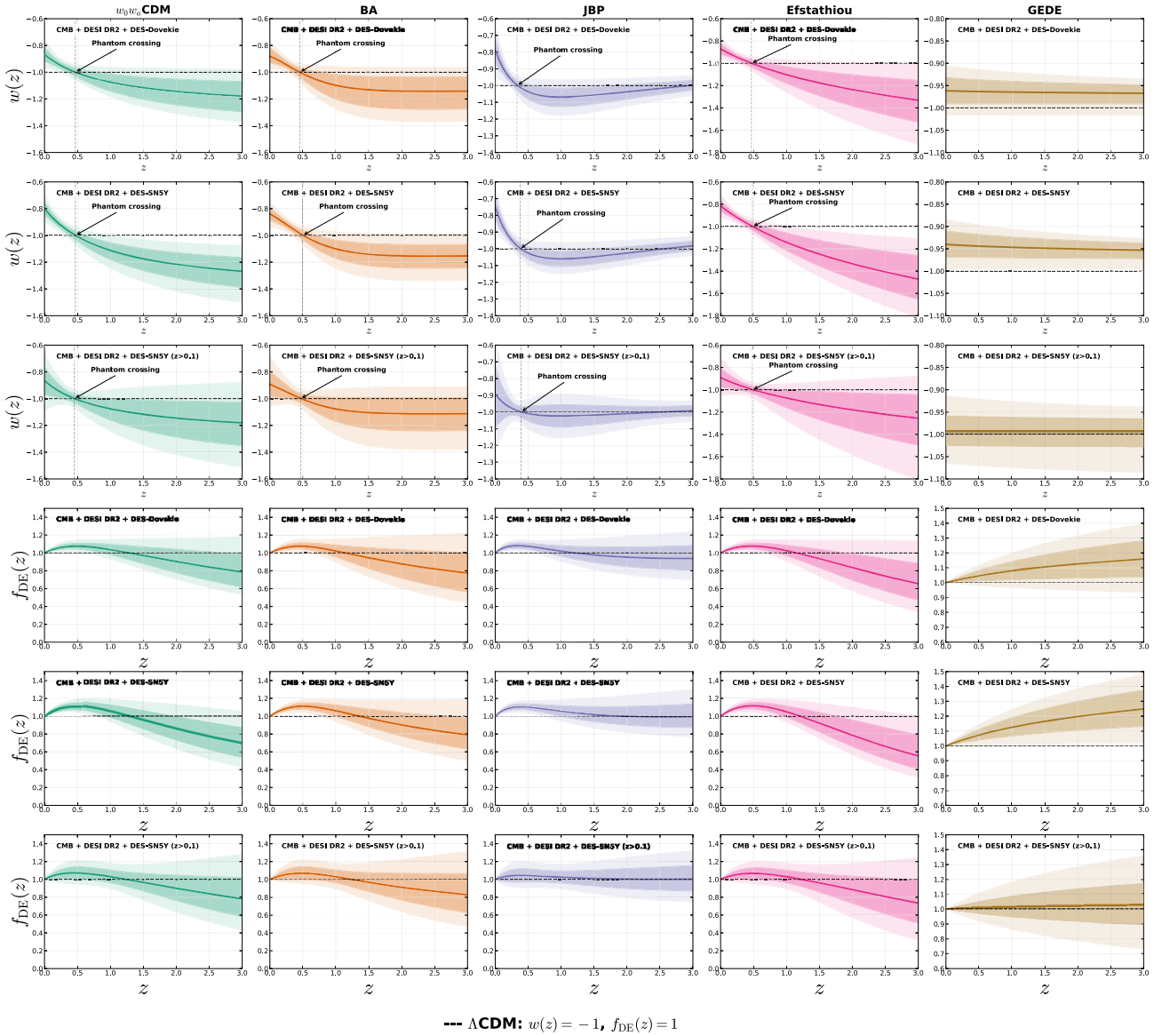


Fig. 2 This figure shows the evolution of the dark energy equation of state $w(z)$ and energy density $f_{\rm DE}(z)$ of w_0w_aCDM, BA, JBP, Efstathiou, and GEDE models as a function of redshift using DESI DR2, combined with the CMB and SNe Ia datasets (DES-Dovekie, DES-SN5Y, and DES-SN5Y ($z > 0.1$)). The solid lines show the mean values, while the light and dark shaded regions correspond to the 1σ and 2σ confidence intervals, respectively

as the null hypothesis. We express the statistical significance in terms of an equivalent Gaussian $N\sigma$, defined through $\mathrm{CDF}_{\chi^2}\left(\Delta\chi^2_{\rm MAP} \,|\, k \text{ dof}\right) = \frac{1}{\sqrt{2\pi}} \int_{-N}^{N} e^{-x^2/2}\, dx$, where k denotes the number of additional parameters of the DDE model relative to ΛCDM.

We observe a clear decrease in the statistical preference for DDE when moving from the DES-SN5Y and DES-SN5Y ($z > 0.1$) datasets to the DES-Dovekie dataset, combined with the CMB compressed likelihood. In particular, the significance reduces from $N\sigma \sim 2.1$–2.4 for DES-SN5Y to below 1σ for DES-Dovekie in each model. For the DES-SN5Y ($z > 0.1$) sample, the significance becomes intermediate between the DES-SN5Y and DES-Dovekie cases, with values in the range $N\sigma \sim 1.1$–1.5. For instance, the wCDM model decreases from 2.12σ to 0σ, while for the DES-SN5Y ($z > 0.1$) sample it becomes 1.50σ, while the w_0w_aCDM, BA, JBP, and Efstathiou parameterizations reduce from $\sim 2.3\sigma$ to $\sim 0.95\sigma$. For the DES-SN5Y ($z > 0.1$) sample, these values become 1.18σ, 1.18σ, 1.09σ, and 1.21σ, respectively. Similarly, the GEDE model shows a drop from 2.15σ to 0.28σ. For the DES-SN5Y ($z > 0.1$) sample, we obtain 1.52σ. This indicates that the preference

for DDE weakens significantly when using the revised DES-Dovekie dataset compared to DES-SN5Y and DES-SN5Y ($z > 0.1$).

4.3 Statistical analysis

Based on the Bayes factor in Efstathiou space reported in Table 1, we show the preference for DDE models relative to ΛCDM using the Jeffreys' scale. For the DES-SN5Y dataset, several models shows the moderate to strong evidence in favor of DDE, with w_0w_aCDM ($\ln \mathcal{B} = 4.87$), BA ($\ln \mathcal{B} = 4.05$), and the Efstathiou parametrization ($\ln \mathcal{B} = 4.40$) showing moderate evidence, while the JBP model ($\ln \mathcal{B} = 5.47$) reaches the threshold for strong evidence. The GEDE model ($\ln \mathcal{B} = 4.03$) also indicates moderate evidence, whereas the wCDM model ($\ln \mathcal{B} = 1.67$) provides only weak evidence.

In contrast, for the DES-Dovekie dataset, the statistical preference for DDE is significantly reduced. Most models fall within the weak to moderate evidence regime, with w_0w_aCDM ($\ln \mathcal{B} = 2.05$), BA ($\ln \mathcal{B} = 1.35$), and the Efstathiou parametrization ($\ln \mathcal{B} = 1.80$) indicating weak evidence, while JBP ($\ln \mathcal{B} = 2.86$) and GEDE ($\ln \mathcal{B} = 2.67$) remain at the lower end of moderate evidence. The wCDM model ($\ln \mathcal{B} = 0.39$) becomes inconclusive. For the DES-SN5Y ($z > 0.1$) dataset, the statistical preference for DDE is further reduced. The w_0w_aCDM ($\ln \mathcal{B} = 0.50$), JBP ($\ln \mathcal{B} = 1.12$), and GEDE ($\ln \mathcal{B} = 1.89$) models shows weak evidence in favor of DDE, while the Efstathiou model ($\ln \mathcal{B} = 0.01$) shows inconclusive evidence in favor of DDE. On the other hand, the wCDM ($\ln \mathcal{B} = -0.18$) and BA ($\ln \mathcal{B} = -0.24$) models show weak evidence in favor of ΛCDM. This comparison demonstrates that the preference for DDE models weakens when transitioning from the DES-SN5Y to the revised DES-Dovekie dataset, while the DES-SN5Y ($z > 0.1$) sample gives intermediate results between the two cases.

4.4 Evolution of the dark energy equation of state $w(z)$ and energy density $f_{DE}(z)$

In Fig. 2, we shows the redshift evolution of the dark energy equation of state $w(z)$ and the density evolution $f_{\rm DE}(z)$ for the w_0w_aCDM, BA, JBP, Efstathiou, and GEDE models. We perform a comparative analysis using the dataset combinations CMB + DESI DR2 + DES-Dovekie, CMB + DESI DR2 + DES-SN5Y, and CMB + DESI DR2 + DES-SN5Y ($z > 0.1$).

We find that, irrespective of whether the DES-SN5Y, DES-SN5Y ($z > 0.1$), and revised DES-Dovekie datasets is used, the combination with DESI DR2 and CMB consistently shows a phantom crossing [53–56]. Specifically, the $w(z)$ predicts $w(z) < -1$ at higher redshifts ($z \gtrsim 0.5$) and transitions to $w(z) > -1$ at lower redshifts ($z \lesssim 0.5$), crossing the $w(z) = -1$. This transition from a non-phantom regime to a phantom regime is characteristic of Quintom-B type behavior. However, the GEDE model shows $w(z) > -1$ throughout its evolution, consistently remaining in the non-phantom regime.

On the other hand, the evolution of $f_{\rm DE}(z)$ for the w_0w_aCDM, BA, JBP, and Efstathiou models shows a characteristic by crossing $f_{\rm DE}(z) = 1$. Specifically, at higher redshifts, these models predicts $f_{\rm DE}(z) < 1$, which then increases and crosses $f_{\rm DE}(z) = 1$, reaching $f_{\rm DE}(z) > 1$ at lower redshifts, and finally converging to $f_{\rm DE}(z) = 1$ at $z = 0$. In contrast, the GEDE model predicts $f_{\rm DE}(z) > 1$ throughout the evolution, while also converging to $f_{\rm DE}(z) = 1$ at $z = 0$.

5 Conclusion

In this work, we investigated whether the preference for DDE found in analyses using the DES-SN5Y supernova sample remains robust after the revision of this dataset into the DES-Dovekie compilation. In addition, we also investigated the impact of removing the very low-redshift supernovae by considering the DES-SN5Y ($z > 0.1$) sample. Motivated by earlier studies based mainly on the w_0w_aCDM framework, we extended the analysis to a broader class of dark energy parametrizations, namely wCDM, w_0w_aCDM, BA, JBP, Efstathiou, and GEDE, using late-time cosmological probes together with the compressed CMB likelihood and DESI DR2 BAO measurements.

Our results show that the DES-SN5Y dataset consistently yields a stronger preference for DDE than the revised DES-Dovekie sample. This trend is visible at the level of parameter constraints, where the DES-SN5Y combination drives the models further away from the ΛCDM limit. In particular, for the redshift-dependent parametrizations, the preferred region is characterized by $w_0 > -1$ and $w_a < 0$, indicating a Quintom-B–type behavior. This corresponds to an evolution in which the dark energy equation of state crosses the phantom divide, with $w(z) < -1$ at earlier times and $w(z) > -1$ near the present epoch. A similar tendency is also reflected in the GEDE model, for which both datasets prefer $\Delta < 0$, with DES-SN5Y showing a stronger departure than DES-Dovekie. For the DES-SN5Y ($z > 0.1$) sample, the same qualitative behavior remains present, although the deviations from the ΛCDM limit become significantly weaker. In particular, the GEDE parameter shifts toward the ΛCDM limit with $\Delta = -0.04 \pm 0.25$, remaining very close to $\Delta = 0$.

At the statistical level, both the $\Delta\chi^2_{\rm MAP}$ analysis and the Bayesian evidence indicate that the preference for DDE weakens significantly when DES-SN5Y is replaced by DES-Dovekie. Using DES-SN5Y, several dynamical models reach

a significance of about 2σ or more relative to ΛCDM, with Bayesian evidence ranging from weak to moderate, and in some cases approaching strong support. By contrast, when the DES-Dovekie dataset is used, the improvement over ΛCDM is substantially reduced, with the frequentist significance dropping below the 1σ level for most models and the Bayesian evidence becoming weak or inconclusive. For the DES-SN5Y ($z > 0.1$) sample, the statistical preference for DDE becomes intermediate between the DES-SN5Y and DES-Dovekie cases, with the significance reducing to about 1.1σ-1.5σ depending on the model, while the Bayesian evidence becomes mostly weak or inconclusive. In some cases, such as the wCDM and BA parametrizations, the Bayesian evidence even slightly favors ΛCDM over the DDE scenarios.

Despite this reduction in statistical significance, an important result of our analysis is that the qualitative behavior of the preferred DDE evolution remains stable across different parametrizations. The tendency toward Quintom-B-like evolution is not exclusive to the w_0w_aCDM model, but appears more generally in BA, JBP, and Efstathiou parametrizations as well. This suggests that the preference seen in DESI DR2 combined with supernova and CMB data is not merely an artifact of one specific parametrization, but may instead point to a broader phenomenological pattern in the late-time expansion history. However, after excluding the very low-redshift ($z < 0.1$) supernovae, the statistical preference for DDE is substantially weakened across all models.

Overall, our findings show that revising DES-SN5Y to DES-Dovekie reduces the statistical preference for DDE, but does not eliminate the underlying trend toward nontrivial dark energy evolution. Similarly, the DES-SN5Y ($z > 0.1$) sample also weakens the preference for DDE compared to the full DES-SN5Y dataset, while still preserving the same qualitative dark energy behavior. Therefore, while the DES-Dovekie sample makes the evidence for DDE less significant than previously inferred from DES-SN5Y, and the DES-SN5Y ($z > 0.1$) sample gives intermediate results between the two cases, the combined late-time data still continue to motivate further investigation of evolving dark energy scenarios beyond the standard ΛCDM model.

Funding P. Channuie has received funding support from the NSRF via the Program Management Unit for Human Resources & Institutional Development, Research and Innovation [grant number B39G690007].

Data Availability Statement Data will be made available on reasonable request. [Authors' comment: The datasets generated during and/or analysed during the current study are available from the corresponding author on reasonable request.]

Code Availability Statement Code/software will be made available on reasonable request. [Authors' comment: The code/software generated during and/or analysed during the current study is available from the corresponding author on reasonable request.]

Open Access This article is licensed under a Creative Commons Attribution 4.0 International License, which permits use, sharing, adaptation, distribution and reproduction in any medium or format, as long as you give appropriate credit to the original author(s) and the source, provide a link to the Creative Commons licence, and indicate if changes were made. The images or other third party material in this article are included in the article's Creative Commons licence, unless indicated otherwise in a credit line to the material. If material is not included in the article's Creative Commons licence and your intended use is not permitted by statutory regulation or exceeds the permitted use, you will need to obtain permission directly from the copyright holder. To view a copy of this licence, visit http://creativecommons.org/licenses/by/4.0/.
Funded by SCOAP[3].

References

1. A.G. Riess et al., Observational evidence from supernovae for an accelerating universe and a cosmological constant. Astron. J. **116**(3), 1009 (1998)
2. S. Perlmutter et al., Measurements of ω and λ from 42 high-redshift supernovae. Astrophys J **517**(2), 565 (1999)
3. C.L. Bennett et al., Nine-Year Wilkinson Microwave Anisotropy Probe (WMAP) Observations: Final Maps and Results. Astrophys. J. Suppl. **208**, 20 (2013)
4. N. Aghanim, et al., Planck 2018 results. I. Overview and the cosmological legacy of Planck, Astron. Astrophys. 641 (2020) A1
5. A. Adame et al., Desi 2024 vi: cosmological constraints from the measurements of baryon acoustic oscillations. J. Cosmol. Astropart. Phys. **2025**(02), 021 (2025)
6. B. Popovic, P. Shah, W. Kenworthy, R. Kessler, T. Davis, A. Goobar, D. Scolnic, M. Vincenzi, P. Wiseman, R. Chen, The dark energy survey supernova program: A reanalysis of cosmology results and evidence for evolving dark energy with an updated type ia supernova calibration (2025), arXiv:2511.07517
7. S. Capozziello, H. Chaudhary, G. Mustafa, S. Pacif, Evidence for dynamical dark energy using desi dr2 lyα forest, arXiv:2510.21976 (2025)
8. S. Capozziello, H. Chaudhary, T. Harko, G. Mustafa, Is dark energy dynamical in the desi era? a critical review. Physics of the Dark Universe , 102196 (2025)
9. Q. Gao, Z. Peng, S. Gao, Y. Gong, On the evidence of dynamical dark energy. Universe **11**(1), 10 (2024)
10. G.-B. Zhao, R.G. Crittenden, L. Pogosian, X. Zhang, Examining the evidence for dynamical dark energy. Phys. Rev. Lett. **109**(17), 171301 (2012)
11. U. Alam, V. Sahni, A.A. Starobinsky, The case for dynamical dark energy revisited. J. Cosmol. Astropart. Phys. **2004**(06), 008–008 (2004)
12. W. Giarè, T. Mahassen, E. Di Valentino, S. Pan, An overview of what current data can (and cannot yet) say about evolving dark energy. Phys. Dark Univ. **48**, 101906 (2025)
13. H. Chaudhary, V.K. Sharma, S. Capozziello, G. Mustafa, Probing Departures from ΛCDM by Late-time Datasets. Astrophys. J. Suppl. **283**(2), 73 (2026)
14. G.-B. Zhao, M. Raveri, L. Pogosian, Y. Wang, R.G. Crittenden, W.J. Handley, W.J. Percival, F. Beutler, J. Brinkmann, C.-H. Chuang et al., Dynamical dark energy in light of the latest observations. Nat. Astron. **1**(9), 627–632 (2017)
15. V.K. Sharma, H. Chaudhary, S. Kolekar, Probing generalized emergent dark energy with desi dr2. Journal of High Energy Astrophysics , 100518 (2025)

16. H. Chaudhary, S. Capozziello, S. Praharaj, S. K. J. Pacif, G. Mustafa, Is the λcdm model in crisis?, Journal of High Energy Astrophysics 100507 (2025)
17. H. Chaudhary, S. Capozziello, V.K. Sharma, G. Mustafa, Does desi dr2 challenge λcdm paradigm? Astrophys. J. **992**(2), 194 (2025)
18. R. Nagpal, H. Chaudhary, H. Gupta, S. Pacif, Late-time constraints on dynamical dark energy models using desi dr2, type ia supernova, and cc measurements. J. High Ener Astrophys. **47**, 100396 (2025)
19. H. Chaudhary, S. Capozziello, V. K. Sharma, I. Gómez-Vargas, G. Mustafa, Evidence for evolving dark energy from desi dr2 bao and pantheon$^+$, des-dovekie, and union3, arXiv:2508.10514 (2025)
20. Z. Zhang, T. Xu, Y. Chen, Dynamical Dark Energy and the Unresolved Hubble Tension: Multi-model Constraints from DESI 2025 and Other Probes. Astrophys. J. **999**(2), 248 (2026)
21. T. Xu, S. Kumar, Y. Chen, A. J. S. Capistrano, Ö. Akarsu, Probing Dynamical Dark Energy with Late-Time Data: Evidence, Tensions, and the Limits of the w_0w_aCDM Framework (2 2026). arXiv:2602.11936
22. E. Abdalla et al., Cosmology intertwined: a review of the particle physics, astrophysics, and cosmology associated with the cosmological tensions and anomalies. JHEAp **34**, 49–211 (2022)
23. E. Di Valentino et al., The CosmoVerse white paper: addressing observational tensions in cosmology with systematics and fundamental physics. Phys. Dark Univ. **49**, 101965 (2025)
24. N. Aghanim, et al., Planck 2018 results. VI. Cosmological parameters, Astron. Astrophys. 641 (2020) A6, [Erratum: Astron.Astrophys. 652, C4 (2021)]
25. L. Balkenhol et al., Measurement of the CMB temperature power spectrum and constraints on cosmology from the SPT-3G 2018 TT, TE, and EE dataset. Phys. Rev. D **108**(2), 023510 (2023)
26. T. Louis et al., The Atacama Cosmology Telescope: DR6 power spectra, likelihoods and ΛCDM parameters. JCAP **11**, 062 (2025)
27. A.G. Riess, W. Yuan, L.M. Macri, D. Scolnic, D. Brout, S. Casertano, D.O. Jones, Y. Murakami, G.S. Anand, L. Breuval et al., A comprehensive measurement of the local value of the hubble constant with 1 km s- 1 mpc- 1 uncertainty from the hubble space telescope and the sh0es team. Astrophys. J. Lett. **934**(1), L7 (2022)
28. S. Weinberg, The Cosmological Constant Problem. Rev. Mod. Phys. **61**, 1–23 (1989)
29. B. Ratra, P.J. Peebles, Cosmological consequences of a rolling homogeneous scalar field. Phys. Rev. D **37**(12), 3406 (1988)
30. R.R. Caldwell, R. Dave, P.J. Steinhardt, Cosmological imprint of an energy component with general equation of state. Phys. Rev. Lett. **80**(8), 1582 (1998)
31. R.R. Caldwell, A phantom menace? cosmological consequences of a dark energy component with super-negative equation of state. Phys. Lett. B **545**(1–2), 23–29 (2002)
32. B. Feng, The quintom model of dark energy (2006), astro-ph/0602156
33. M. Chevallier, D. Polarski, Accelerating universes with scaling dark matter. Int. J. Modern Phys. D **10**(02), 213–223 (2001)
34. E.V. Linder, Exploring the expansion history of the universe. Phys. Rev. Lett. **90**(9), 091301 (2003)
35. E. Barboza Jr., J. Alcaniz, A parametric model for dark energy. Phys. Lett. B **666**(5), 415–419 (2008)
36. H. Jassal, J. Bagla, T. Padmanabhan, Wmap constraints on low redshift evolution of dark energy. Mon. Notices R. Astron. Soc. **356**(1), L11–L16 (2005)
37. A. Tripathi, A. Sangwan, H. Jassal, Dark energy equation of state parameter and its evolution at low redshift. J. Cosmol. Astropart. Phys. **2017**(06), 012 (2017)
38. X. Li, A. Shafieloo, Evidence for emergent dark energy. Astrophys. J. **902**(1), 58 (2020)
39. A. Gelman, D.B. Rubin, Inference from Iterative Simulation Using Multiple Sequences. Stat. Sci. **7**, 457–472 (1992)
40. A. Lewis, GetDist: a Python package for analysing Monte Carlo samples. JCAP **08**, 025 (2025)
41. M.A. Karim, J. Aguilar, S. Ahlen, S. Alam, L. Allen, C.A. Prieto, O. Alves, A. Anand, U. Andrade, E. Armengaud, Desi dr2 results. ii. measurements of baryon acoustic oscillations and cosmological constraints. Phys. Rev. D **112**(8), 083515 (2025)
42. N. Aghanim, et al., Planck 2018 results. vi. cosmological parameters, Astron. Astrophys 641 A6 (2020)
43. T. Abbott, M. Acevedo, M. Aguena, A. Alarcon, S. Allam, O. Alves, A. Amon, F. Andrade-Oliveira, J. Annis, P. Armstrong, The dark energy survey: Cosmology results with 1500 new high-redshift type ia supernovae using the full 5-year dataset (2024), arXiv:2401.02929
44. D. Brout et al., The Pantheon+ Analysis: Cosmological Constraints. Astrophys. J. **938**(2), 110 (2022)
45. Y. Chen, S. Kumar, B. Ratra, T. Xu, Effects of Type Ia Supernovae Absolute Magnitude Priors on the Hubble Constant Value. Astrophys. J. Lett. **964**(1), L4 (2024)
46. B. Popovic, et al., The Dark Energy Survey Supernova Program: A Reanalysis Of Cosmology Results And Evidence For Evolving Dark Energy With An Updated Type Ia Supernova Calibration (11 2025). arXiv:2511.07517
47. R.E. Kass, A.E. Raftery, Bayes Factors. J. Am. Stat. Assoc. **90**(430), 773–795 (1995)
48. R. Trotta, Bayes in the sky: Bayesian inference and model selection in cosmology. Contemp. Phys. **49**, 71–104 (2008)
49. Y. Cai, X. Ren, T. Qiu, M. Li, X. Zhang, The quintom theory of dark energy after desi dr2, National Science Review. nwag115 (2026)
50. G. Gu, X. Wang, Y. Wang, G.-B. Zhao, L. Pogosian, K. Koyama, J.A. Peacock, Z. Cai, J.L. Cervantes-Cota, M. Ishak et al., Dynamical dark energy in light of the desi dr2 baryonic acoustic oscillations measurements. Nat. Astron. **9**(12), 1879–1889 (2025)
51. B. Feng, X. Wang, X. Zhang, Dark energy constraints from the cosmic age and supernova. Phys. Lett. B **607**(1–2), 35–41 (2005)
52. P. Thanankullaphong, P. Sahoo, P.H. Puttasiddappa, N. Roy, Quintom dark energy: Future attractor and phantom crossing in light of desi dr2 observation (2026), arXiv:2601.02284
53. E. Özülker, E.D. Valentino, W. Giarè, Dark energy crosses the line: Quantifying and testing the evidence for phantom crossing (2025), arXiv:2506.19053
54. E. Silva, R.C. Nunes, Testing signatures of phantom crossing through full-shape galaxy clustering analysis. J. Cosmol. Astropart. Phys. **2025**(11), 078 (2025)
55. Z. Yao, G. Ye, A. Silvestri, A general model for dark energy crossing the phantom divide. J. Cosmol. Astropart. Phys. **2025**(10), 078 (2025)
56. D. Efstratiou, E.A. Paraskevas, L. Perivolaropoulos, Addressing the desi dr2 phantom-crossing anomaly and enhanced h_0 tension with reconstructed scalar-tensor gravity (2025), arXiv:2511.04610
57. K. Lodha, A. Shafieloo, R. Calderon, E. Linder, W. Sohn, J. Cervantes-Cota, A. De Mattia, J. García-Bellido, M. Ishak, W. Matthewson et al., Desi 2024: Constraints on physics-focused aspects of dark energy using desi dr1 bao data. Phys. Rev. D **111**(2), 023532 (2025)
58. K. Lodha, R. Calderon, W. Matthewson, A. Shafieloo, M. Ishak, J. Pan, C. Garcia-Quintero, D. Huterer, G. Valogiannis, L. Ureña-López, Extended dark energy analysis using desi dr2 bao measurements (2025), arXiv:2503.14743